Electronic Supplementary Material (ESI) for CrystEngComm.

Crystal growth and structural remarks in malonate-based lanthanide coordination polymers

Fernando S. Delgado, Pablo Lorenzo-Luís, Jorge Pasán, Laura Cañadillas-Delgado, Oscar Fabelo, María Hernández-Molina, Antonio D. Lozano-Gorrín, Francesc Lloret, Miguel Julve and Catalina Ruiz-Pérez*

---

[a] *Laboratorio de Rayos X y Materiales Moleculares (MATMOL), Departamento de Física, Facultad de Ciencias (Sección Física), Universidad de La Laguna, Avda. Astrofísico Francisco Sánchez s/n, E-38204 La Laguna, Tenerife, Spain. E-mail: caruiz@ull.ull.es*

[b] *Departamento de Química, Facultad de Ciencias (Sección Química), Universidad de La Laguna, Avda. Astrofísico Francisco Sánchez s/n, E-38204 La Laguna, Tenerife, Spain.*

[c] *Centro Universitario de la Defensa de Zaragoza, Ctra. Huesca s/n, 50090, Zaragoza, Spain*

[d] *Institut Laue Langevin, Diffraction Group, 71 Rue des Martyrs, 38008, Grenoble, France.*

[e] *Departamento de Ingeniería, Escuela Superior de Ingeniería, Universidad de La Laguna, Avda. Astrofísico Francisco Sánchez s/n, E-38204 La Laguna, Tenerife, Spain.*

[f] Instituto de Ciencia Molecular (ICMol), Universitat de València, C/ Catedrático José Beltrán 2, 46980 Paterna, València, Spain.

*Corresponding author. E-*mail:* caruiz@ull.ull.es

CONTENTS

Results and discussion

Section Crystal structures:

Section Powder X-ray diffraction study:

The PXRD patterns were collected at room temperature. The Rietveld refinement [see **reference 19** on the manuscript] which was carried out on each of the patterns corresponds to the fitting of the full structure. The program used to perform these refinements was the Fullprof [see **reference 20** on the manuscript]. A pseudo-Voigt function was used to describe the peak shape whereas a polynomial function with five refinable coefficients was employed to define the background.

Figure 13 on the manuscript shows observed (red) and calculated (black) PXRD patterns for (a) **1a**, (b) **1d**, (c) **2** and (d) **2a** after fitted using the Rietveld method. The lower part of the figure (green) shows the difference between the observed and calculated plots, and the vertical marks (blue) are the reflections allowed by the corresponding space group for the malonate-based polymer. By looking at the difference plot corresponding to (a), (b), (c), and (d), one can realize that those for compounds (c) and (d) do not look that great due to the loss of statistics in the PXRD pattern for those two compounds with respect to (a) and (b) (observe the number of counts of intensity for (a) and (b) and for (c) and (d)), under the same measurement conditions. This loss of statistics is also visible through the increase on the agreement factors (R) for (c) and (d) respect to (a) and (b).

Figure S1. Observed (red) and calculated (black) X-ray diffraction patterns for (a) **1**, (b) **1b**, and (c) **1c** after fitted using the Rietveld method. The lower part of the figure (green) shows the difference between observed and calculated plots, and the vertical marks (blue) are the reflections allowed by the corresponding space group for the malonate-based polymer.

Section Thermal analysis:

Figure S2. Thermal analysis of [Ln$_2$(mal)$_3$(H$_2$O)$_5$]·2H$_2$O [Ln = Tb (**1a**), Dy (**1b**), Er (**1c**) and Yb (**1d**); mal = malonate], [Sm$_2$(mal)$_3$(H$_2$O)$_6$] (**2**) and [Ce$_2$(mal)$_3$(H$_2$O)$_3$]·2H$_2$O (**4·2H$_2$O**).

***Section Preparative routes and structural remarks on malonate-based lanthanide(III) CPs*:**

Solvent evaporation method. This technique requires several conditions: (a) saturated solutions for the crystal growing; (b) the solubility increasing with the temperature and so, the crystals can be formed during the cooling step.

Hydro(solvo)thermal method. This method exploits the self-assembly of products from soluble precursors. It was originally used for the synthesis of zeolites, but it has been adapted to the synthesis of MOFs. The operational temperature range is 80–260 °C inside a closed container in an autoclave under autogenously pressure. This can be influenced mainly by the speed of the cooling rate at the end of the reaction.

Table S1. Selected Bond Lengths (Å) for $\mathbf{1\cdot 2H_2O}$[a, b]

Holmium coordination sphere

Ho(1)-O(1)	2.843(4)	Ho(1)-O(11)	2.307(4)
Ho(1)-O(2)	2.363(4)	Ho(1)-O(1w)	2.366(6)
Ho(1)-O(2w)	2.346(6)	Ho(1)-O(3w)	2.343(6)
Ho(2)-O(1)	2.377(4)	Ho(2)-O(12c)	2.318(4)
Ho(2)-O(21)	2.313(4)	Ho(2)-O(4w)	2.404(6)
Ho(2)-O(5w)	2.366(6)		

Hydrogen bonds

D-H···A	D···A/Å	D-H···A	D···A/Å
O(1w)-H···O(6wf)	2.755(9)	O(4w)-H···O(11c)	2.740(5)
O(1w)-H···O(6wg)	2.755(9)	O(4w)-H···O(11d)	2.740(5)
O(2w)-H···O(22h)	2.691(7)	O(5w)-H···O(6wi)	2.790(8)
O(2w)-H···O(22e)	2.691(7)	O(5w)-H···O(6wj)	2.790(8)
O(3w)-H···O(21)	2.771(5)	O(6w)-H···O(2)	2.842(9)
O(3w)-H···O(21a)	2.771(5)	O(6w)-H···O(22h)	2.796(9)

[a] Symmetry codes: (a) x, $-y-1/2$, z; (b) x, $-y+1/2$, z; (c) $x-1/2$, $-y+1/2$, $-z-1/2$; (d) $x-1/2$, y, $-z-1/2$; (k) $x+1/2$, $-y-1/2$, $-z-1/2$; (f) $-x+1$, $-y$, $-z+1$; (g) $-x+1$, $y-1/2$, $-z-1$; (h) $x+1/2$, y, $-z-1/2$; (i) $-x+1$, $-y$, $-z-1$; (j) $-x+1$, $y+1/2$, $-z-1$. [b] A = acceptor; D = donor. [c] Symmetry operators apply to acceptor atoms

Table S2. Selected Bond Lengths (Å) for $\mathbf{2\cdot 2H_2O}$[a b]

Samarium coordination sphere

Sm(1)-O(1)	2.371(4)	Sm(1)-O(11)	2.549(4)
Sm(1)-O(2)	2.427(4)	Sm(1)-O(12)	2.602(4)
Sm(1)-O(4b)	2.321(4)	Sm(1)-O(12a)	2.448(3)
Sm(1)-O(1w)	2.532(4)	Sm(1)-O(2w)	2.504(5)
Sm(1)-O(3w)	2.484(4)		

Hydrogen bonds

D-H···A	D···A/Å	D-H···A	D···A/Å
O(1w)-H···O(3g)	2.715(8)	O(1w)-H···O(11h)	2.839(7)
O(2w)-H···O(3i)	2.756(8)	O(2w)-H···O(2wj)	2.827(11)
O(3w)-H···O(1i)	2.791(6)	O(3w)-H···O(2a)	2.733(9)

[a] Symmetry transformations: (a) $-x-1/2$, $-y-1/2$, $-z+1$; (b) $-x-1/2$, $y-1/2$, $-z+1/2$. [b] Symmetry operators apply to acceptor atoms

Table S3. Selected Bond Lengths (Å) for **3·2H$_2$O**$^{a\ b}$

Cerium coordination sphere			
Ce(1)-O(1)	2.461(3)	Ce(1)-O(11)	2.557(3)
Ce(1)-O(2)	2.481(4)	Ce(1)-O(12)	2.729(3)
Ce(1)-O(4b)	2.436(4)	Ce(1)-O(12a)	2.502(3)
Ce(1)-O(1w)	2.557(3)	Ce(1)-O(2w)	2.507(4)
Ce(1)-O(3w)	2.557(4)		

Hydrogen bonds^{b}

D-H···A	D···A/Å	D-H···A	D···A/Å
O(1w)-H···O(4w)	2.747(6)	O(1w)-H···O(3f)	2.693(5)
O(2w)-H···O(3w)	2.656(6)	O(2w)-H···O(4b)	2.983(5)
O(3w)-H···O(1g)	2.756(5)	O(3w)-H···O(2h)	2.684(5)

^{a} Symmetry transformations: (a) $–x, -y, -z-1$; (b) $–x+1/2, y-1/2, z$. ^{b} A = acceptor; D = donor. ^{c} Symmetry operators apply to acceptor atoms.

Table S4. Selected Bond Lengths (Å) for **4·2H$_2$O**^{a,b}

Cerium coordination sphere			
Ce(1)-O(1)	2.576(6)	Ce(1)-O(11)	2.638(6)
Ce(1)-O(3)	2.463(6)	Ce(1)-O(12)	2.682(6)
Ce(1)-O(7)	2.453(6)	Ce(1)-O(1w)	2.527(6)
Ce(1)-O(9b)	2.741(7)	Ce(1)-O(2w)	2.618(7)
Ce(1)-O(10b)	2.601(7)	Ce(1)-O(3w)	2.552(7)
Ce(2)-O(1)	2.565(7)	Ce(2)-O(6d)	2.445(6)
Ce(2)-O(2)	2.616(6)	Ce(2)-O(8d)	2.531(6)
Ce(2)-O(3a)	2.534(6)	Ce(2)-O(9)	2.451(7)
Ce(2)-O(4a)	2.695(7)	Ce(2)-O(12)	2.543(6)
Ce(2)-O(5)	2.391(7)		

Donor····Acceptor distances D····A (Å)^{b}

D····A	D····A/Å	D···A	D···A/Å
O(1w)····O(7)	2.970(6)	O(3w)····O(6d)	2.752(7)
O(1w)····O(11)	2.975(7)	O(3w)····O(8e)	3.029(6)
O(1w)····O(2h)	2.704(6)	O(3w)····O(9b)	2.771(7)
O(2w)····O(3)	2.994(7)	O(1wC)····O(2w)	2.859(7)
O(2w)····O(7)	2.737(8)	O(1wC)····O(7)	2.946(8)
O(2w)····O(5b)	3.079(7)	O(1wC)····O(8)	3.028(8)
O(2w)····O(9b)	2.876(7)	O(1wC)····O(10g)	2.799(7)
O(2w)····O(10b)	2.899(7)	O(2wC)····O(1W)	2.794(7)
O(2w)····O(2wCb)	2.837(8)	O(2wC)····O(4f)	2.746(7)
O(3w)····O(3)	3.044(6)	O(2wC)····O(11g)	2.844(7)
O(3w)····O(11)	2.926(6)	O(2wC)····O(2wa)	2.837(8)

^{a} Symmetry transformations: (a) $–1+x, y, z$; (b) $1+x, y, z$; (c) $–x, -1/2+y, 2-z$; (d) $–x, 1/2+y, 2-z$; (e) $1–x, 1/2+y, 2-z$; (f) $–1+x, y, –1+z$; (g) $–x, -1/2+y, 1-z$; (h) $x, y, –1+z$. ^{b}Symmetry operators apply to acceptor atoms.

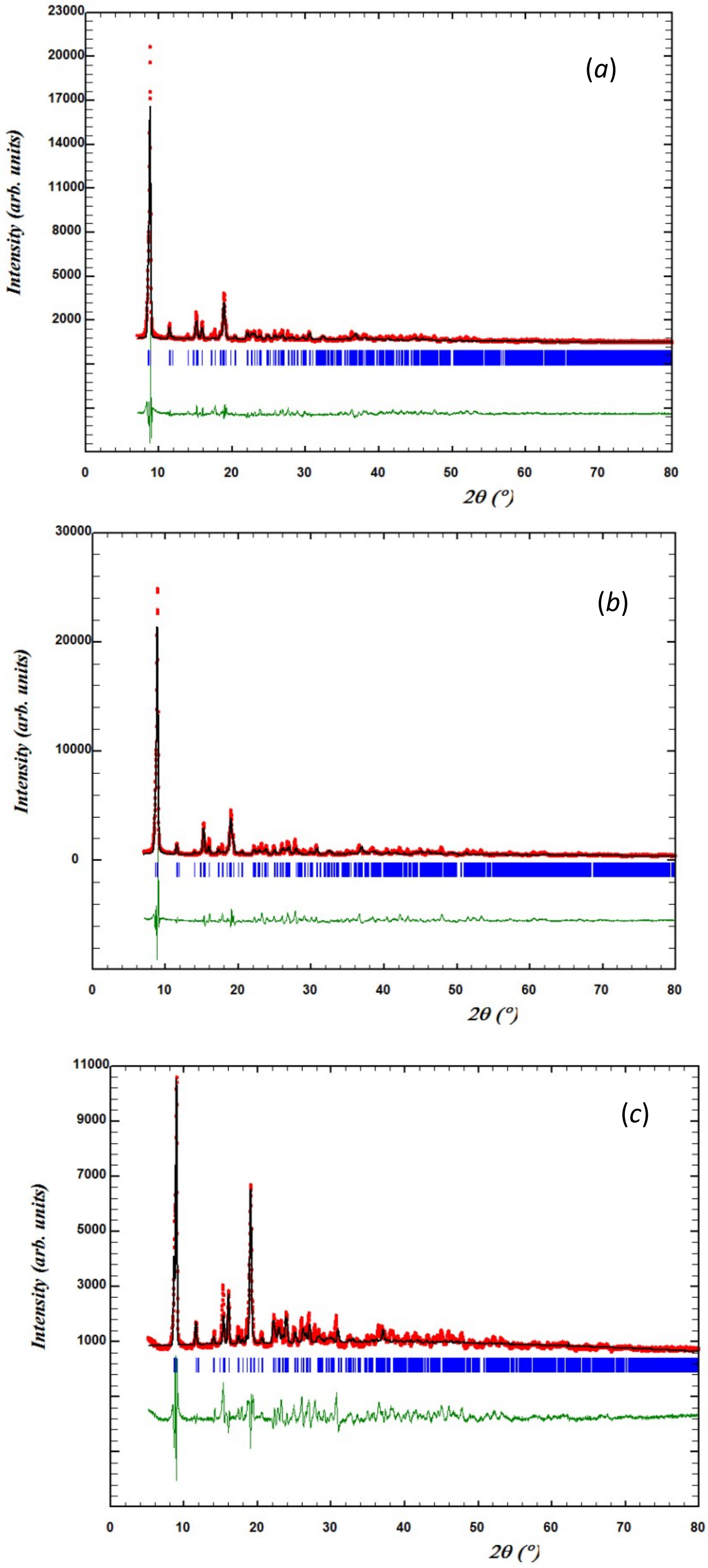

Figure. S1. Observed (red) and calculated (black) X-ray diffraction patterns for (*a*) **1**, (*b*) **1b**, and (*c*) **1c** after fitted using the Rietveld method. The lower part of the figure (green) shows the difference between observed and calculated plots, and the vertical marks (blue) are the reflections allowed by the corresponding space group for the malonate-based polymer.

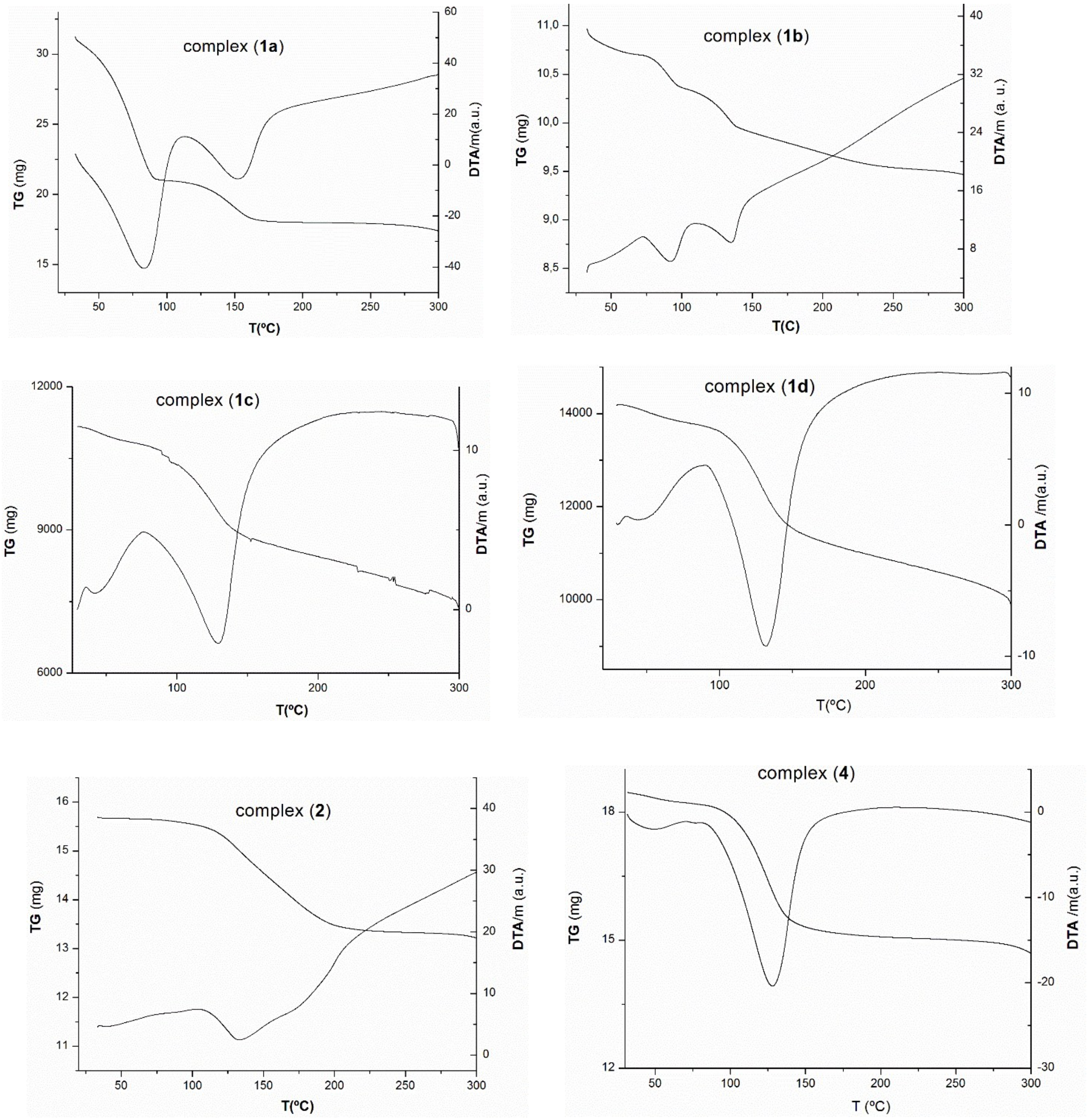

Figure. S2. Thermal analysis of $[Ln_2(mal)_3(H_2O)_5]\cdot 2H_2O$ [Ln = Tb **1a**, Dy **1b**, Er **1c** and Yb **1d**; mal = malonate], $[Sm_2(mal)_3(H_2O)_6]$ **2** and $[Ce_2(mal)_3(H_2O)_3]\cdot 2H_2O$ **4·2H₂O**.